Simulation of dynamic compaction of metal powders

D. Roshan Kumar, R. Krishna Kumar, and P. K. Philip

Simulation of dynamic compaction of metal powders

D. Roshan Kumar, R. Krishna Kumar,[a] and P. K. Philip

Manufacturing Engineering Section, Department of Mechanical Engineering, Indian Institute of Technology, Madras 600 036, India

This article presents numerical studies on the deformation of particles during dynamic compaction of metal powders. The analysis of the process is based on a micromechanics approach using multiple particle configurations. The material considered is elastoviscoplastic with interparticle friction. Two-dimensional studies on particles in close packed arrangement were carried out using plane strain conditions for deformation and thermal response. The finite element method using an explicit dynamic analysis procedure was used for the simulations. The influence of speed of compaction, strain hardening, strain rate dependency, interparticle friction and size of the powder particles on the final shape and temperature variations within the particles were analyzed. The studies offer useful information on the shape and temperature variations within the particles. The results provide a better understanding of the dynamic compaction process at the micromechanics level. © *1999 American Institute of Physics.* [S0021-8979(99)02502-5]

I. INTRODUCTION

Dynamic compaction of metal powders has gained in importance in recent years with the need to improve the properties of compacts obtained through the powder metallurgy route. The technique is attractive as it provides near-net-shaped components with higher green strength, more uniform green density distribution, lower ejection loads, and improved dimensional accuracy.[1,2] Dynamic compaction is effected by passing through the powder an intense shock wave generated by detonating an explosive surrounding the powder, or by the impact of a high velocity projectile. These short duration, large amplitude stress waves propagating through the material cause compaction and bonding of the powder particles. Stress wave interactions with the powder particles are difficult to understand, especially while describing the deformation behavior of the particles from the micromechanics level. Under dynamic compaction, the behavior is largely rate dependent and the inertial loads, which depend on the intensity of the stress wave, must be considered. This article attempts to study the densification behavior of the particles during dynamic compaction at the micromechanics level using a finite element method.

Gourdin[3] provides a detailed review and assessment of both experimental and analytical techniques on dynamic compaction of metal powders. The initial density, stress intensity, stress duration, release waves, dynamic plastic behavior, and the thermal properties of the material affect the final properties of the compact.[4] It is well recognized that the densification of the metal powder is caused by the plastic deformation of the metal powder particles. This plastic deformation causes intense dissipation of plastic work, which is converted to heat. The temperature rise due to this plastic work can even cause localized melting.[5] The increase in the green strength of the dynamically compacted specimen is due to the higher temperature and contact pressures that develop during the process.[6]

There have been very interesting experimental and numerical observations of the dynamic compaction process.[7,8] The change in the morphology of the powder particles from near hexagonal to a concave shape has been observed in a number of studies.[9,10] Though the kinematics of the material compaction was explored to a certain extent by Gourdin,[11] numerical studies using Eulerian finite difference code has thrown more light on the formation of such shapes. Williamson[12] used this technique elegantly to bring out certain important factors, such as the temperature distribution and nonuniform energy dissipation, the effects of simple variation in the initial particle geometry and the mechanics of the consolidation of bimodal particle distribution. He used an elastic perfectly plastic material law and considered the geometry comprising a few particles. Interparticle friction and strain hardening were not used in these models, nor was the formation of the particle shape investigated in detail.

In the current work, a particle level finite element analysis of the process was done using a commercial explicit code ABAQUS. A rate dependent model (elastoviscoplastic) depicts the behavior of the powder particle, and interparticle friction was also taken into consideration. The temperature rise was calculated by considering the process as adiabatic. This work clearly brings out the mechanics of compaction and the effect of process and material parameters.

II. MODEL AND ANALYSIS PROCEDURE

The usual dynamic compaction process involves closed die compaction by pressing the metal powder inside the die cavity at higher compaction rates. Basically, there are two approaches for simulation of the process. The first method treats the powder based on the principles of continuum mechanics and studies the mechanism as a whole, while the second studies the process at the micromechanics level. The

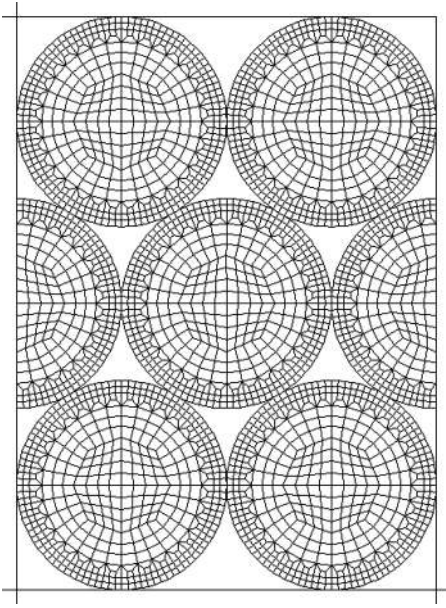[a]Author to whom all the correspondence should be addressed; electronic mail: rkrkumar@hotmail.com

FIG. 1. Finite element model with top, bottom, and side plates.

TABLE I. Process and material parameters used for numerical simulations.

Compaction speed m/s	300, 500, 1000
Interparticle friction coefficient	0.01, 0.1, 0.2, 0.3
Viscosity parameter β/s	10, 40, 1000, 2000
Over stress power law index n	4, 5
Strain hardening E_T kN/mm^2	0.0, 0.2
Particle size in microns	50, 100, 200

current work involves numerical simulation in which a few powder particles and voids around them are explicitly modeled. A closely packed arrangement of steel particles of 100 μm size was considered for the analysis. Figure 1 shows the initial configuration and the finite element discretization of the model used. The model consists of seven particles arranged in close contact with one another and comprises 2880 quadrilateral elements with 3195 nodes. Each particle consists of 480 elements and 529 nodes. The top plate, the base plate, and the side walls were modeled as rigid bodies with contact conditions specified at all interface regions. The simulations were performed as two dimensional plane strain analysis. Inspite of the limitations of two-dimensional analysis, the model is capable of predicting many important aspects of the compaction process. Due to the short time period of the process, adiabatic heat transfer analysis was performed thereby neglecting conductive and radiative heat transfer.[12]

The material considered was elastoviscoplastic with Young's modulus $=200$ GPa, initial yield strength $=215$ MPa, Poisson's ratio$=0.3$, specific heat$=0.42\times10^3$ J/kg K. During dynamic loading conditions, the inelastic behavior of the material exhibits rate dependence and the flow stress increases, hence a viscoplastic model is essential for the analysis. The strain rate dependency was incorporated in the analysis using the overstress power law expressed as

$$\mathbf{D}^{\mathrm{pl}}=\beta\left\{\frac{\bar{\sigma}}{\sigma_y}-1\right\}^n \quad \text{for} \ \bar{\sigma}\geqslant\sigma_y, \tag{1}$$

where $\mathbf{D}^{\mathrm{pl}}$ is the plastic part of the strain rate tensor, $\bar{\sigma}$ the yield strength at nonzero plastic strain, and σ_y the initial yield strength. β and n are the material properties. The yield strength $\bar{\sigma}$ depends on the strain hardening property of the material. It is obtained using the tangent modulus value, which defines the strain hardening behavior of the material.

The shear stress transfer across the particle interfaces was provided through frictional contact and incorporated in the analysis using the Coulomb friction model. This is based on the principle that two contacting surfaces can carry shear stresses up to a certain magnitude across their interface before slipping relative to each other. The model assumes that no relative motion occurs if the equivalent frictional stress is less than the critical stress, which is expressed as $\tau_{\mathrm{crit}}=\mu p$, where p is the contact pressure and μ the coefficient of friction. The critical shear stress determines whether a contact point is in slipping or sticking condition.

The top punch was displaced downwards in a short duration of time thereby simulating the dynamic loading process. The analysis was performed at different compaction speeds and material properties. The various process and material parameters considered for the analysis are shown in Table I. The influence of speed of compaction, strain hardening, strain rate dependency, interparticle friction, and size of the powder particles on the final shape and temperature variations within the particles were analyzed.

The simulations were performed as a nonlinear explicit dynamic analysis procedure including adiabatic analysis using the general-purpose finite element package ABAQUS/EXPLICIT. The method of explicit analysis is computationally efficient and used a large deformation theory which allows the model to undergo large displacements and rotations.[13,14] The explicit dynamic analysis procedure is based upon the implementation of an explicit integration rule using a diagonal lumped mass matrix. The explicit central difference operator satisfies the dynamic equilibrium equations at the beginning of the increment, the accelerations, calculated at time t using mass matrix and the residual. This is used to calculate the velocity at time $t+\Delta t/2$ and the displacement at $t+\Delta t$. The number of operations involved is equal to the number of equations because the lumped mass matrix is diagonal and the equations are uncoupled. The equilibrium equations of motion of a material point in an explicit scheme can be expressed as

$$\ddot{\mathbf{u}}^{(i)}=\mathbf{M}^{-1}(\mathbf{F}^{(i)}-\mathbf{I}^{(i)}), \tag{2}$$

where $\mathbf{M}$ is the diagonal lumped mass matrix, $\mathbf{F}$ is the applied load vector, and $\mathbf{I}$ the internal force vector. The following relations are used for the calculation of velocity and displacement

$$\dot{\mathbf{u}}^{(i+1/2)}=\dot{\mathbf{u}}^{(i-1/2)}+[(\Delta\mathbf{t}^{(i+1)}+\Delta\mathbf{t}^{(i)})/2]\ddot{\mathbf{u}}^{(i)} \tag{3}$$

$$\mathbf{u}^{(i+1)}=\mathbf{u}^{(i)}+\Delta t^{(i+1)}\dot{\mathbf{u}}^{(i+1/2)}, \tag{4}$$

where **u** is the displacement, **u̇** the velocity, and **ü** the acceleration. The superscript ''i'' refers to increment number, (i $-1/2$) and ($i+1/2$) refer to the mid increment values.

Once the displacement field is obtained, the strain and stress fields can be easily calculated. The central difference operator is explicit in that the kinematic state may be advanced using the known value of $\dot{\mathbf{u}}^{(i-1/2)}$ and $\ddot{\mathbf{u}}^{(i)}$ from the previous increment. The analysis may take an extremely large number of increments, but each increment is relatively inexpensive and results in an economical solution. The explicit analysis is ideally suited for the simulation of high speed events such as dynamic compaction process.

III. RESULTS AND DISCUSSION

A. Speed of compaction

When a material is stressed with a suddenly applied load, the progress of the stress in the material is in the form of stress waves. Its velocity is a characteristic of the material and the amplitude depends on the intensity of the load applied. This type of loading has been simulated by displacing the top plate downwards through a distance of 30, 40, and 50 μm in time periods of 100, 80, and 50 ns, corresponding to compaction speeds of 300, 500, and 1000 m/s, respectively. For each compaction speed, the displacement and time for displacement of the top plate are such that the stress waves during compaction reach beyond the middle portion of the lower layer of particles and the simulation stops before the stress waves reach the bottom plate and are reflected back.

The material considered was elastic perfectly viscoplastic with rate dependency parameters $\beta=40$ and $n=4$. The interparticle friction coefficient was considered as 0.01. Studies were concentrated on the deformation behavior of the center particle of the model whose deformation is affected only by contact pressures developed through the surrounding particles. It is well established that during quasistatic compaction, deformation occurs by the development of plastic strains from the interparticle contact locations and spreads towards the interior of the particles forming a hexagonal shaped configuration.[15,16] But, as can be seen from this work, during dynamic compaction, the plastic strains develop from the loading end and spread through each layer of particles in the direction of the stress wave propagation. The intensity and the speed of the propagating stress wave which, in turn, depend on the compaction speed, influence the deformation of the particles. The final configuration of the particles obtained by dynamic compaction at speeds of 300, 500, and 1000 m/s are shown in Fig. 2. At compaction speeds of 300 m/s, the particle shape is near hexagonal as in case of quasistatic compaction. But at a compaction speed of 1000 m/s, the particle shape is convex on the upstream side of the shock propagation direction and concave on the downstream side.

The curved shape can be explained by observing the material velocity variations and the corresponding plastic strain developments within the particles at different stages during dynamic compaction. As the stress wave propagates downwards, the material attains higher velocities and plastically deforms. The presence of voids causes different mate-
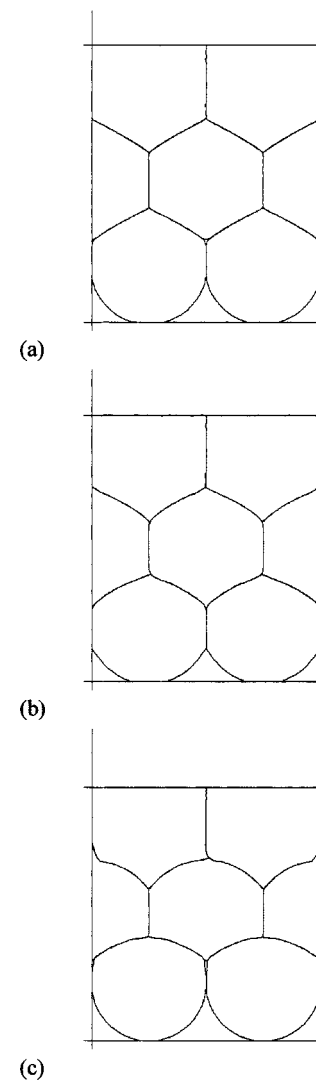

FIG. 2. Particle configuration attained at different speeds of compaction. (a) 300, (b) 500, and (c) 1000 m/s.

rial speeds within the particle. The velocity distributions within the center particle and the bottom two particles of the initial configuration were analyzed to understand the kinematics of the shape formation. The magnitude and direction of the material velocities at different stages during compaction at speed of 1000 m/s are shown in Fig. 3. It can be observed from Figs. 3(a)–3(c) that as the stress wave propagates downward, the deformation starts from this region. On reaching the surface of the particles near the voids, the stress waves lead to an increase in the material speed, as the voids offer less resistance to the flow of material in that region. Figure 3(d) shows that at the point where the stress wave propagates to the next layer of particles, the material velocities at the lower sides of the top particle are very high compared to the material speeds within the top layer of the lower particles. This causes the lower layer particles to behave to a certain extent like a rigid body. Hence, the top particle deforms on to the top of the lower particles and takes the concave shape. As the stress propagates further down [Fig. 3(e)], the interstitial voids are filled up by material extrusion and the peak is formed as observed in the microstructure inves-
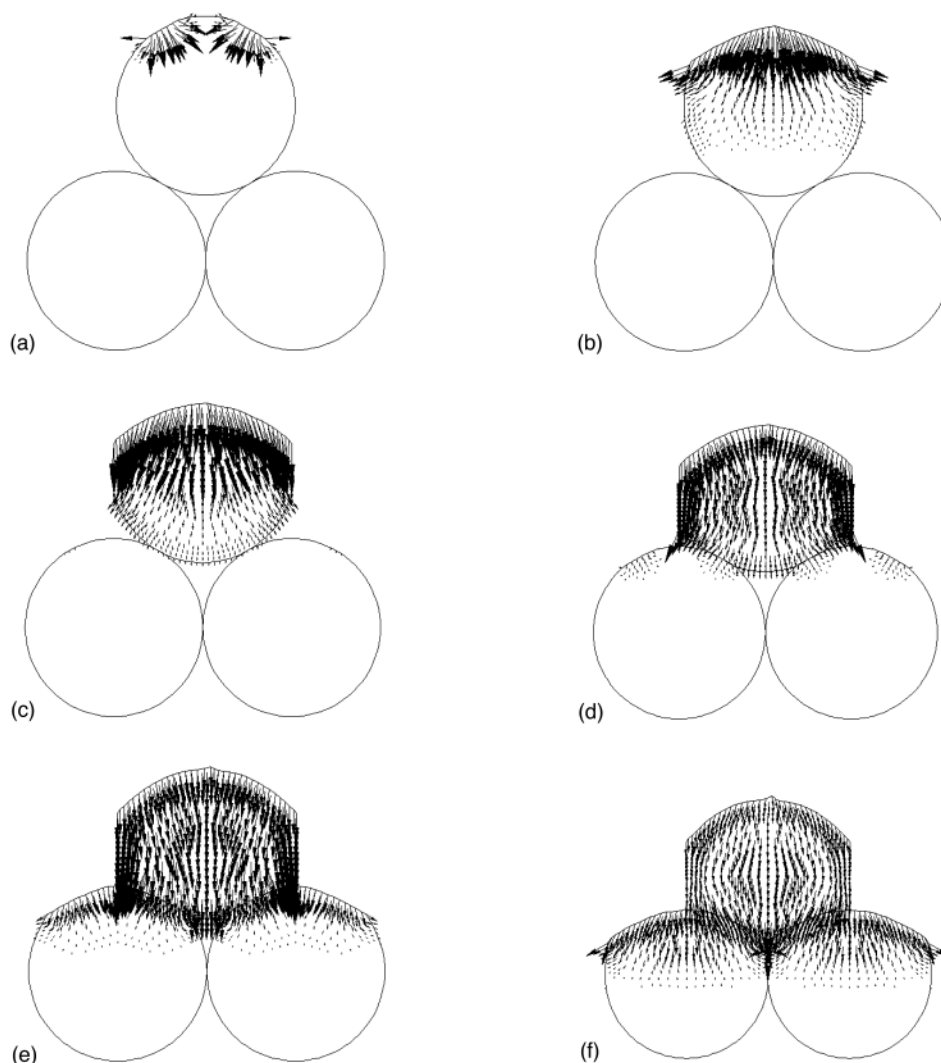
FIG. 3. Material velocities at different stages during compaction at speed of 1000 m/s. (a) Time, $t=20$ ns, max. velocity, $v=347$ m/s, (b) $t=30$ ns, $v=1316$ m/s, (c) $t=35$ ns, $v=1294$ m/s, (d) $t=40$ ns, $v=2169$ m/s, (e) $t=45$ ns, $v=2214$ m/s, and (f) $t=50$ ns, $v=3665$ m/s.

tigations reported earlier.[11] At later stages [Fig. 3(f)], the particles move downward as a whole and the shape formed remains unaltered.

The above phenomenon can also be observed clearly by examining the development of plastic deformation. The material velocities occurring in the particles due to the stress waves cause plastic deformation. Figure 4 shows the equivalent plastic strain development at different stages at a compaction speed of 1000 m/s. Plastic strains develop from the top and spread downwards in the direction of the stress propagation. Figures 4(a)–4(c) show the spread of plastic strains during the initial stages of compaction. Figure 4(d) shows the stage where the lower particles have attained only very low plastic strains when compared to the strains in the top particle. This causes the top particle to deform plastically on top of the lower particles [Fig. 4(e)]. Further, the top particle plastically deforms and fills the interstitial voids, thereby forming a sharp peaked structure on the lower part of the particles. The plastic strain development pattern correlates well with the velocity distributions described earlier.

On the other hand, when the compaction speeds are lower, strains develop at the interparticle contact region as in the quasistatic process. At a compaction speed of 300 m/s, due to the propagation of the stress wave from the region of loading, the plastic strains spread downwards. Strains at the interparticle contact regions also increase simultaneously, as in the case of quasistatic compaction but at a lower magnitude. Figure 5 shows the equivalent plastic strain development at various stages during dynamic compaction at 300 m/s. Figure 5(a) shows the spread of plastic strains downwards from the top and Fig. 5(b) shows further spread of plastic strains and the subsequent development of strains at the interparticle contact regions. Figures 5(c) and 5(d) show the spread of plastic strains further downwards and the simultaneous increase of strain at the interparticle contact region thereby increasing the particle contact lengths. Figure 5(e) shows the instant at which the strains spread to the next layer of particles and when the interparticle contact lengthens. The further spread of the plastic strain is shown in Fig.
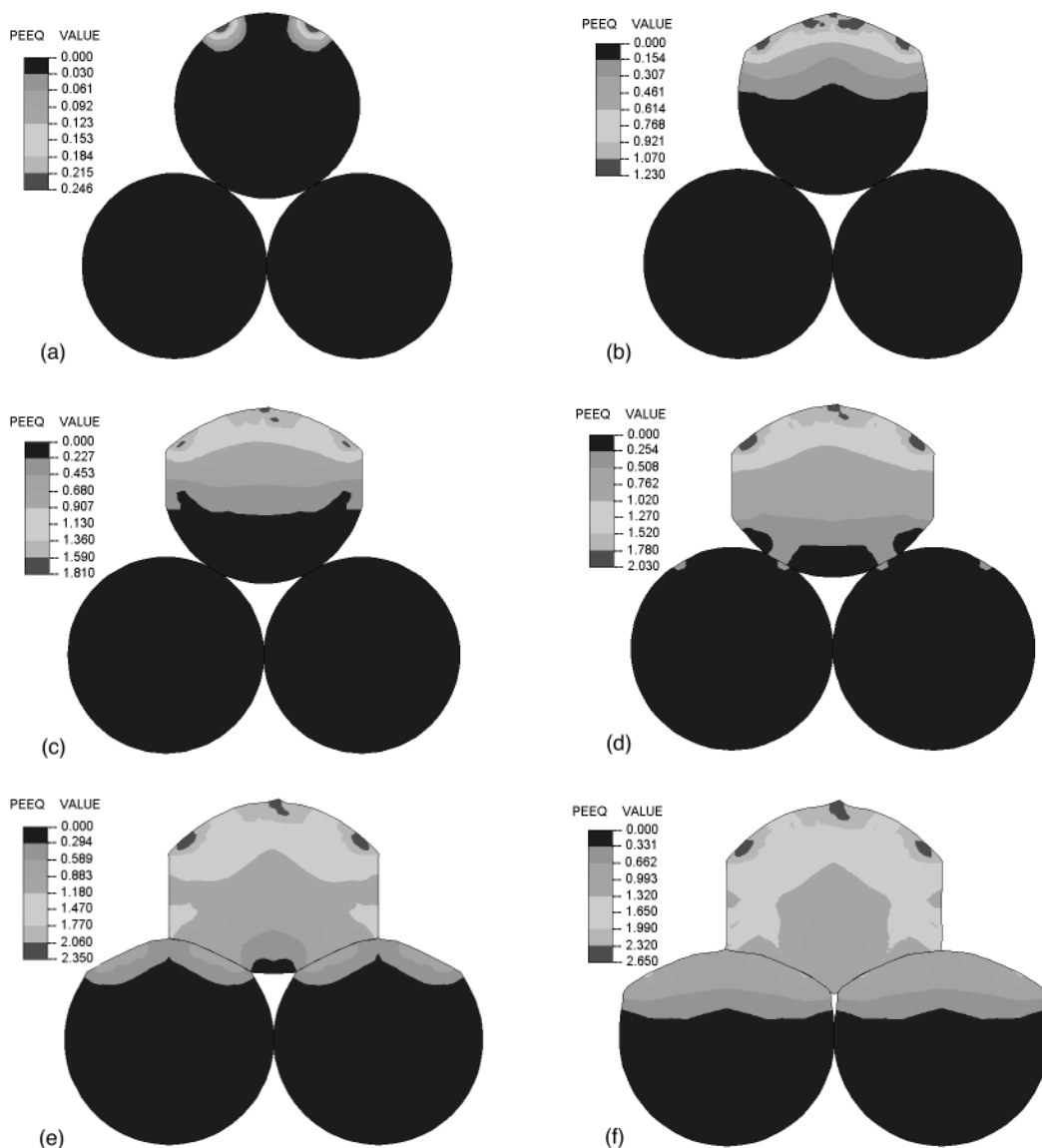
FIG. 4. Equivalent plastic strain development at different stages during compaction at speed of 1000 m/s. (a) 20, (b) 30, (c) 35, (d) 40, (e) 45, and (f) 50 ns.

5(f). This explains the formation of hexagonal shape of the particles at lower speeds of compaction.

The strain rate dependency of the material has been incorporated in the analysis by using the overstress power law as expressed in Eq. (1). The effect of rate dependency on the particle shape formation was studied by varying the rate dependency material parameters ''β'' and ''n''. Figure 6 shows the final configuration at compaction speed of 500 m/s with $\beta = 40$ and $n = 5$. It may be observed that the particles have acquired a concave shape. The shape of the particles at identical conditions and with $n = 4$ is seen to be hexagonal [Fig. 2(b)]. Hence, it can be inferred that with an increase in the value of n, the rate dependency of the material reduces and the particles change from hexagonal to curved shape. The effect of viscosity parameter β on the particle shape was further analyzed by varying the value at 10, 1000, and 2000, with $n = 4$ at compaction speed of 500 m/s. The final configurations obtained are shown in Fig. 7. At $\beta = 10$, the shape is hexagonal but with higher values of 1000 and 2000, the material becomes less rate dependent and the particle shape

changes to concave. These results bring out the effect of rate dependency of the material on the final shape of the particles during dynamic compaction.

B. Temperature variations

The passing of stress waves through the powder particles generates intense plastic deformation, mainly at the periphery of the particles. The combination of this plastic deformation and friction between particle raises the temperature as a consequence of adiabatic heating. This raises the preferential heating of the particle surfaces to high temperature, which can even lead to localized melting. However, the adiabatically heated material cools rapidly due to the heat flow towards the core of the particle, which is at relatively lower temperature level. The compaction speeds and material properties of the powder influence the magnitude and the location of these high temperature regions. Figure 8 shows the temperature variations within the center particle of the model at different speeds of compaction. Higher temperatures have
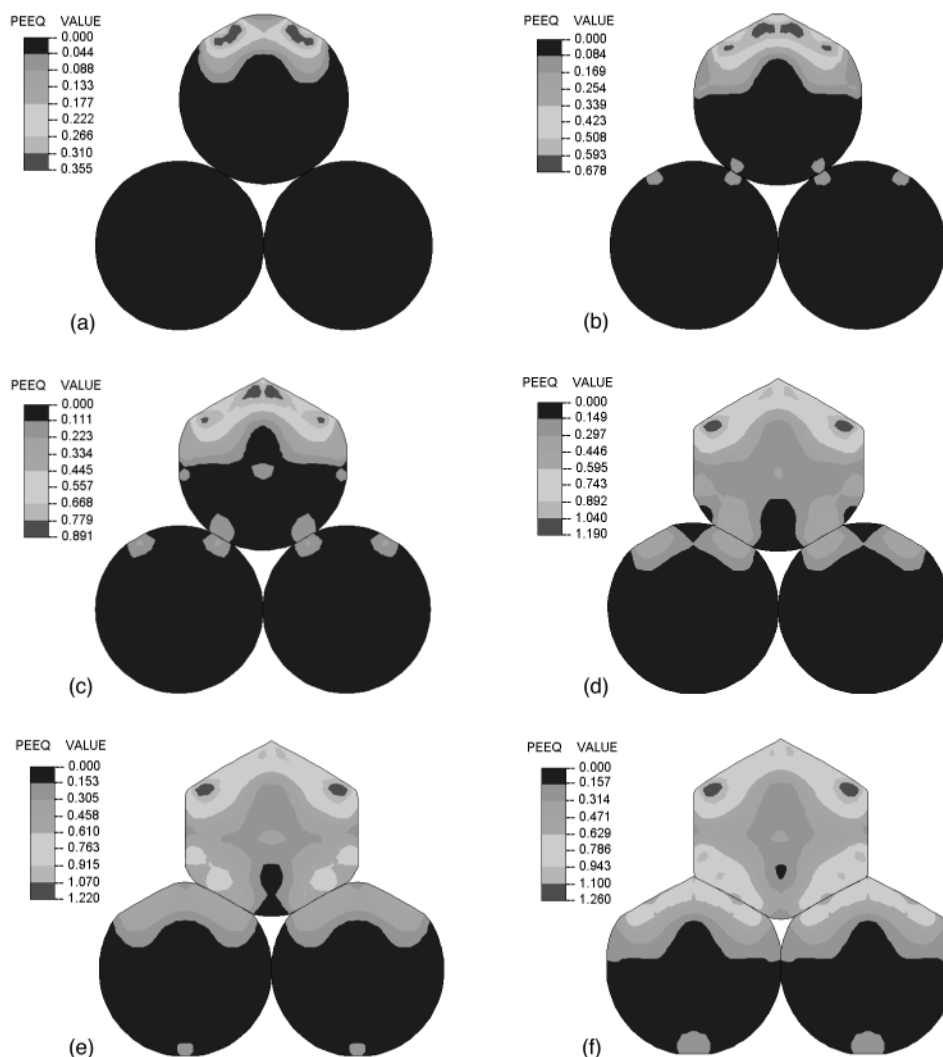
FIG. 5. Equivalent plastic strain development at different stages during compaction at speed of 300 m/s. (a) 40, (b) 60, (c) 70, (d) 80, (e) 90, and (f) 100 ns.

been observed on the particle surface near the void regions in the initial configuration. This can be attributed to the higher velocities and contact pressures at these locations and, hence, the surface temperature rises with the increase in compaction speed. The temperature variations on the surface of the particle near the void region, where it was maximum, observed during compaction at various speeds are shown in Fig. 9. At higher compaction speeds, it was observed that the surface temperature increases high enough to cause localized melting and, hence, form strong interparticle bonds. Figure 10 shows the temperature variations at the interior of the particle during compaction at different speeds. The interior attains relatively low temperature compared to the surface.

The effect of rate dependency of the material on the temperature variations within the particles was also studied. The temperature variations within the center particle at a compaction speed of 500 m/s with rate dependency parameters $\beta=40$ and $n=5$ were analyzed. As discussed earlier, increasing the value of n reduces the rate dependency of the material and hence the temperature can be expected to be lower. Compared with identical conditions and $n=4$ [Fig. 8(b)], it was observed that the maximum surface temperature within the particle drops from 2850 to 2300 K and the inte-

rior temperature from 1100 to 711 K. The effect of parameter β on the temperature variation within the particle at a compaction speed of 500 m/s was further analyzed. The increase in β value reduces the rate dependency of the material, and the temperature attained also drops. With $\beta=10$, 1000, and 2000, the maximum surface temperature attained is 4860, 2120, and 1860 K, respectively, and the interior temperature 1580, 700, and 593 K.
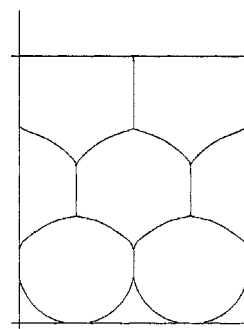

FIG. 6. Particle configuration at compaction speed of 500 m/s with rate dependency parameters $\beta=40$ and $n=5$.
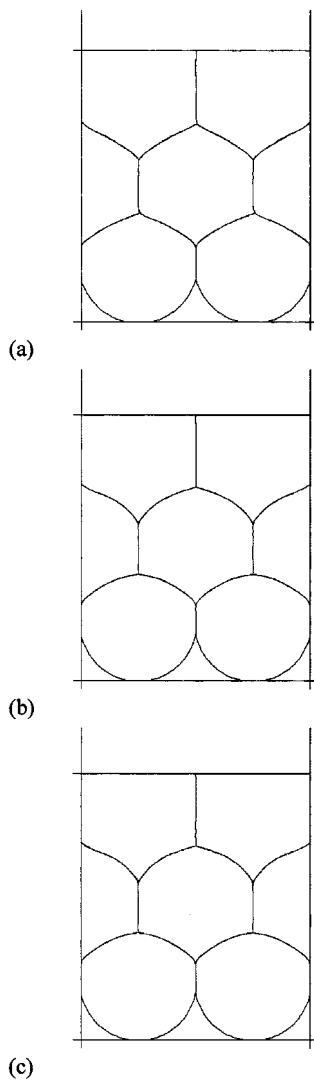
FIG. 7. Particle configuration at compaction speed of 500 m/s with rate dependency parameters $n=4$, and (a) $\beta=10$, (b) $\beta=1000$, and (c) $\beta=2000$.

FIG. 8. Temperature contours within the center particle at different speeds of compaction (a) 300, (b) 500, and (c) 1000 m/s.

C. Interparticle friction

The friction between particles is controlled greatly by the irregularities and the texture of the particle surface. Under dynamic conditions, interparticle friction increases due to the particles shearing past one another at high speeds in contrast to the quasistatic loading conditions.[17] Numerical studies were performed using the original model with friction coefficients of 0.01, 0.1, 0.2, and 0.3. The temperature profile obtained within the center particle for different friction values were observed to be similar except for magnitude at the higher temperature locations. Figure 11 shows the temperature variations at the maximum temperature region on the surface of the particles at a compaction speed of 500 m/s for different friction coefficients. Temperature increases on the surface of the particle have been observed for higher friction values. At a friction value of 0.01, the surface temperature reached 1604 K, whereas for a friction value of 0.3, the temperature rises to 2730 K.
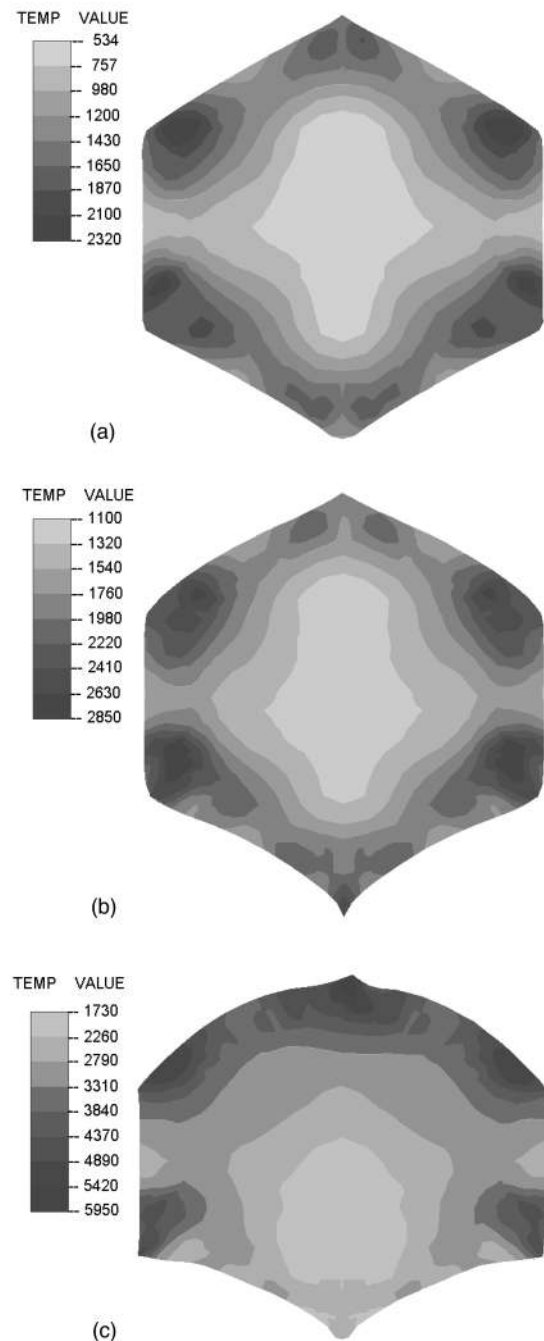
D. Effect of strain hardening

The powder particle behavior following dynamic loading may also depend on the strain hardening properties of the material. To understand this effect, the material was considered elastoviscoplastic with strain hardening. A tangent modulus E_T of 0.2 kN/mm^2 was introduced to the original model and studies were performed at compaction speeds of 300, 500, and 1000 m/s. The final shape of the particles and temperature variations obtained were analyzed. At a speed of 300 m/s, the shape is hexagonal and at 1000 m/s the shape changes to concave. The results reveal that the final configuration remains approximately the same as without strain
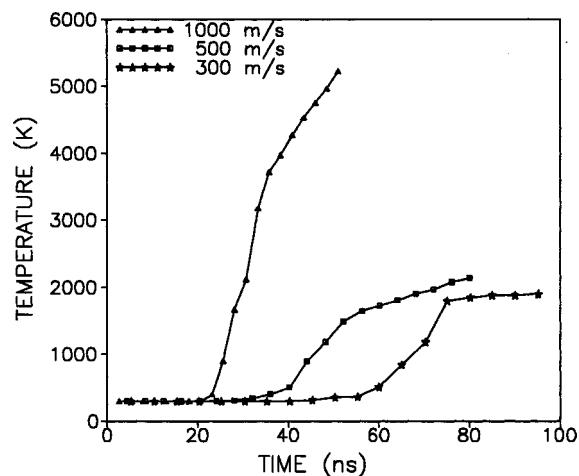
FIG. 9. Temperature variations at the maximum temperature region on the surface of the particle during compaction at speeds of 300, 500, and 1000 m/s.

FIG. 11. Temperature variations at the maximum temperature region on the surface of the particle during compaction at speed of 500 m/s for different interparticle friction values.

hardening, and the particle temperature profiles are also identical though the magnitude of the surface temperature is observed to be higher. At 300 m/s, the maximum temperature attained was 3760 K but at compaction speed of 1000 m/s, it reached as high as 9000 K. From the results, it can be concluded that the strain hardening properties of the material do not alter the shape of the particle but increases the surface temperature of the particles at different speeds of compaction.

E. Effect of particle size

Studies were further extended to analyze the effect of variations in the particle size. Finite element models were created with similar configuration as in the initial case with particle sizes of 50 and 200 μm. Numerical experiments were performed on these models considering the material as elastic perfectly viscoplastic at compaction speed of 500 m/s. It was observed from the results that the final configuration of the particles remains almost identical for different particle sizes of 50, 100, and 200 μm. Plastic strains were observed
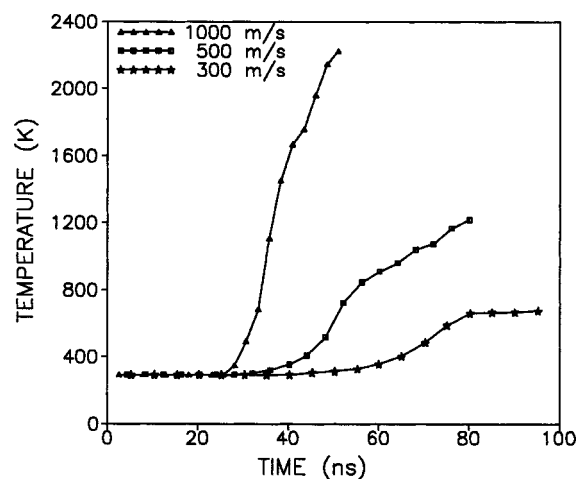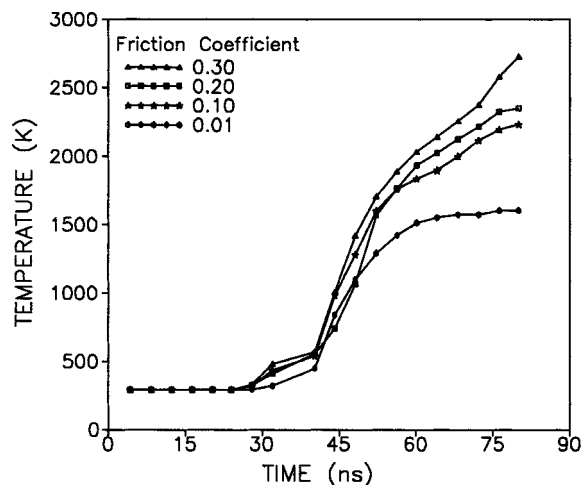
to increase as the size of the particle reduced and the surface temperature rose correspondingly. With a particle size of 50 μm, the peak temperature attained at the surface was 3770 K whereas with 200 μm size particle, the maximum surface temperature attained was 2240 K.

IV. CONCLUSIONS

Dynamic compaction process has been simulated and discussed based on particle level studies. A variety of numerical experiments has been conducted to provide an insight into the behavior of the particles under such loading conditions. The deformation pattern and temperature variations within the particle at different process and material parameters have been analyzed. At higher speeds of compaction, the particles attain a convex shape at the top portion and concave shape with sharp peaks at the lower part. The kinematics of the formation of this particular shape has been explained by the increase in material velocities near the void regions as the deformations take place. Localized high temperature regions are observed on the particle surfaces, which depend on such parameters as compaction speed, interparticle friction, rate dependency, strain hardening, and size of the particles. The temperature increase is of primary importance as it causes interparticle welding and provides better strength for the dynamically compacted parts.

ACKNOWLEDGMENTS

FIG. 10. Temperature variations at interior of the particle during compaction at speeds of 300, 500, and 1000 m/s.

[1] N. W. Page and P. D. Killen, Powder Metall. **30**, 233 (1987).
[2] B. M. Butcher and C. H. Karnes, J. Appl. Phys. **40**, 2967 (1969).
[3] W. H. Gourdin, Prog. Mater. Sci. **30**, 39 (1986).
[4] P. Kasiraj, T. Vreeland, Jr., R. B. Schwarz, and T. J. Ahrens, Acta Metall. **32**, 1235 (1984).
[5] G. Alvarez, A. C. Gonzalez, and J. C. Cuyas, Powder Metall. **32**, 53 (1986).
[6] D. G. Morris, Mater. Sci. Eng. **57**, 187 (1983).

[7] J. E. Flinn, R. L. Williamson, R. A. Berry, R. N. Wright, Y. M. Gupta, and M. Williams, J. Appl. Phys. **64**, 1446 (1988).
[8] H. Matsumoto and K. I. Konda, J. Mater. Sci. **24**, 4042 (1989).
[9] R. N. Wright, G. E. Korth, and J. E. Flinn, Metall. Trans. A **20A**, 2449 (1989).
[10] D. J. Benson and W. J. Nellis, Appl. Phys. Lett. **65**, 418 (1994).
[11] W. H. Gourdin, Mater. Sci. Eng. **67**, 179 (1984).
[12] R. L. Williamson, J. Appl. Phys. **68**, 1287 (1990).

[13] Hibbitt, Karlsson and Sorensen, Inc., ABAQUS Theory Manual ver. 5.5 (1995), p. 2.4.5-1.
[14] K. J. Bathe, in *Finite Element Procedures* (Prentice Hall, India, 1996), p. 824.
[15] Ch. P. Chand and R. K. Kumar, Scr. Mater. **35**, 767 (1996).
[16] Ch. P. Chand and R. K. Kumar, Acta Metall. Mater. **45**, 1425 (1997).
[17] M. Yosuff and N. W. Page, Powder Technol. **76**, 299 (1993).